# A Refined Prediction Method for the Unsteady Aerodynamics of Supersonic Elastic Aircraft

JACK MORITO II*
*The Boeing Company, Seattle, Wash.*

**This paper interprets the inaccuracies arising from the Mach box evaluation of unsteady aerodynamic forces based on the method of Aerodynamic Influence Coefficients (AIC), and proposes refinements to minimize these inaccuracies. The basic equations of inviscid flow are reviewed and the assumptions and restrictions inherent in present application of the AIC method are discussed. The inaccuracies, which result in large fluctuations of the pressure distribution, stem primarily from distortion of the leading edge which results from a Mach box grid representation of the wing planform. The refinement consists of a subdivision of the grid of pulse-sending boxes while maintaining the original grid of pulse-receiving box control points. Numerical examples are included to demonstrate its efficiency. The downwash singularity near a subsonic leading edge is also considered and a numerical procedure for evaluating its effect is shown.**

## Nomenclature

$A$ = integrated area and integration constant
$a$ = speed of sound
$a_j$ = amplitude of the $j$th mode oscillation
$b_r$ = reference length
$b_1$ = chordwise dimension of Mach box
$k_1$ = reduced frequency based on $b_1$, $k_1 = \omega b_1/U$
$L$ = lift force
$M$ = Mach number in uniform flow condition
$N$ = subdivision factor
$P$ = pressure
$Q_{ij}$ = Generalized force for the $i$th elastic mode and loading for the $j$th mode
$U$ = uniform flow speed $= Ma$
$u, v, w$ = perturbation velocities in $x$, $y$ and $z$ components
$z_i(x, y)$ = $i$th mode shape
$z(x, y, t)$ = displacement of a point $(x, y)$ in $z$ direction at time $t$
$\alpha_D$ = deepness of subsonic (supersonic) leading edge
$\alpha^{m,n}$ = area ratio over the $(m, n)$ edge box
$\beta$ = $(M^2 - 1)^{1/2}$
$\rho$ = air density
$\xi, \eta, \zeta$ = dummy coordinate in $x$, $y$ and $z$ axes
$\tau$ = dimensionless time, $\tau = Ut/b_1$
$\phi$ = velocity potential function
$\omega$ = circular fequency
$\Delta\phi$ = velocity potential difference

*Subscripts*

$i$ = $i$th mode
$o$ = nontime dependent quantity
$si$ = leading edge singularity starting at $i$
$t.$ or $t.e$ = trailing edge
$l.$ or $l.e$ = leading edge
$\nu\mu$ = box $(\nu, \mu)$

*Superscripts*

$k_i$ = Aerodynamic Influence Coefficient (AIC) based on the reduced fequency, $k_i$
$m, n$ = box $(m, n)$
$\bar{(\ )}$ = dimensionless quantity
$(D)$ = values over diaphragm region
$i$ = $i$th mode

Presented as Paper 70-944 at the AIAA Guidance, Control and Flight Mechanics Conference, Santa Barbara, Calif., August 17–19, 1970; submitted September 28, 1970; revision received May 19, 1971. The author acknowledges and appreciates the contributions made by W. S. Rowe.

* Senior Engineer, Commerical Airplane Group. Member AIAA.

## Introduction

THE numerical evaluation of linearized aerodynamic loading in unsteady supersonic inviscid flow is most effectively achieved in the low-to-moderate supersonic range by using the aerodynamic influence coefficient method of lifting surface theory (abbreviated AIC), first proposed by Pines, Dugundji, et al.[1,2]

It is well known, however, among aerodynamicists that this AIC method of applying the numerical box scheme may produce highly inaccurate chordwise and spanwise pressure fluctuations, even though its performance on some generalized force computations is acceptable. Earlier estimations that accuracy could be improved by use of a finer box grid are in error because the pressure fluctuations merely increase in spatial frequency, but do not decrease in amplitude.

The principal finding of these studies is that the highly irregular pressure fluctuations are produced by a) the singular nature of the AIC's along the forward Mach lines emanating from receiving point, b) strong upwash which is discontinuous at a subsonic leading edge and in the opposite direction on the diaphragm ahead of the edge, and c) the irregular points† produced by the multibox jagged leading edge of a grid of boxes. These effects combine to cause noticable fluctuations in the velocity potential distributions which when differentiated cause the pressure distribution to oscillate unrealistically chordwise and spanwise over the wing planform.

Various schemes have been tried for reducing the irregular pressure fluctuations. A least-squares surface fit method[4] when applied to the velocity potential distribution yields smooth pressure distributions. The basic fluctuations in the velocity potential curves are averaged out, but are not theoretically corrected. The other technique that has been applied is the use of correction factors which scale the velocity potentials by exact solution values obtained for steady-state constant angle of attack for all modes and reduced frequencies.[1] It is felt that this procedure is not truly valid, since for nonzero frequencies the potentials are complex, and there is no theoretical guarantee that the potential distributions for high order modes resemble that for a constant pitching mode.

The present analytically-motivated approach to the reduction of spurious pressure fluctuations consists of the following schemes:

1) The box grid is subdivided into a finer grid system in odd increments. The new subboxes are used as pulse-sending

† The irregular points are defined as the downstream corners of regions where the leading edge cuts more than one box on the chordwise or spanwise strips.

regions while the original grid of pulse-receiving points, so-called control points, is maintained.

2) Subdivision is not applied to the whole area. There is introduced the concept of effective area which slides from row-to-row in a streamwise direction and may contain approximately the same number of subdivided boxes as the number of original boxes required in the solution.

3) A numerical singularity is distributed along subsonic leading and side edges to more accurately simulate the physical flow field near the plan-form boundary.

4) The velocity potential functions corrected by the subdivision technique are further smoothed by a least-squares error fit method in both spanwise and chordwise directions.

5) A refined area rule scheme, which relocates the local box lift to the area centroid of a cut box, is included.

Results obtained through both the refined and conventional techniques are compared with exact solutions for $k_1 = 0$, and also presented for cases where $k_1 \neq 0$.

## Review of Thin Airfoil Theory in Supersonic Flow

Thin airfoil or small perturbation theory is applied to describe the flow patterns that result when small disturbances are superposed on parallel uniform flow. When coordinate axes are fixed on a thin body placed in uniform flow, the perturbation velocity potential satisfies the differential equation.

$$(1 - M^2)\phi_{xx} + \phi_{yy} + \phi_{zz} - (2M/a)\phi_{xt} - (1/a^2)\phi_{tt} = 0 \quad (1)$$

Equation (1) can be transformed into a canonical form of the wave equation which is always hyperbolic and whose general solution is known. By transforming back to the body coordinate system, the general solution will be,

$$\phi(x, y, z, t) = (A/r)\{f(t - \tau_1) + f(t - \tau_2)\} \quad (2)$$

where

$$r = (1/\beta^2)[(x - \xi)^2 - \beta^2\{(y - \eta)^2 + (z - \zeta)^2\}]^{1/2} \quad (3a)$$

$$\tau_1 = (M/a)[(x - \xi)/\beta^2] - r/a \quad (3b)$$

$$\tau_2 = (M/a)[(x - \xi)/\beta^2] + r/a \quad (3c)$$

Consider a lifting surface whose leading edge is supersonic (for convenience the $y$ axis is placed on the leading edge), so that there is no communication between the upper and lower surfaces (see Fig. 1). The potential at $P(x, y, z)$ and at time $t$ is computed from a source singularity distribution over the $x, y$ plane and is

$$\phi(x, y, z, t) = \int_0^{x-z} d\xi \int_{y-\eta_0}^{y+\eta_0} \frac{A(\xi, \eta, \zeta)}{r} \{f(t - \tau_1) + f(t - \tau_2)\} d\eta \quad (4)$$

where

$$\eta_0 = \{[(x - \xi)^2/\beta^2] - (z - \zeta)^2\}^{1/2}$$

$$A(\xi, \eta, 0+) = -(1/2\pi\beta^2) W_0(\xi, \eta, 0+) \quad (5)$$

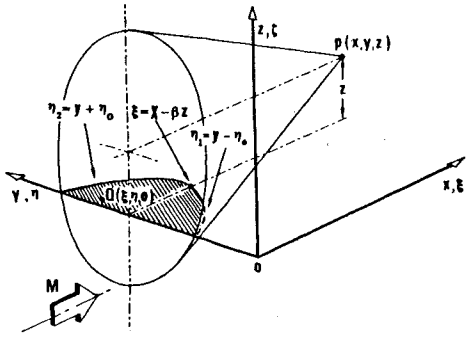


**Fig. 1 Distributed singularities on planar surface with supersonic leading edge.**

where $W_0$ is the nontime-dependent part of the upwash $w$. If the time variation $f(t)$ of the source singularity is harmonic, then

$$f(t) = e^{i\omega t} \quad (6)$$

By substitution of Eqs. (5) and (6) into Eq. (4) and by letting $z \to 0$, the potential at the plane of the surface can now be obtained, as,

$$\lim_{z \to 0+} \phi(x, y, z, t) =$$

$$-\exp(i\omega t)/\pi \iint_A W_0(\xi, \eta, 0+) \times \frac{\exp[-i\omega M(x - \xi)/a\beta^2]\cos(\omega R/a\beta^2)}{R_h} d\xi d\eta \quad (7)$$

where $A$ = area bounded by the wing leading edge and the forward Mach lines emanating from a pulse-receiving point $(x, y, 0+)$; $R_h$ = Hyperbolic radius $= \beta^2 r = [(x - \xi)^2 - \beta^2(y - \eta)^2]^{1/2}$. From the previous discussion, Eq. (7) is only valid for harmonically oscillating source singularities in which the wing leading edges are supersonic.

## A Study of Aerodynamic Influence Coefficient Method in Box Grid Systems

If the integration area $A$ may be split into sufficiently small elementary areas, one may make approximations in the evaluation of the double integral in Eq. (7). Assuming that the upwash over a unit box area is uniform, the potential difference at the center of box $(m, n)$ denoted as $\Delta\phi(x_m, y_n)$ may be written symbolically as:

$$\Delta\phi(x_m, y_n) = \sum_\nu \sum_\mu W_0(\xi, \eta) \times \underbrace{\left\{ b_r \iint_{A(\nu, \mu)} \frac{\exp[-ik_r M^2(\bar{x}_m - \bar{\xi})/\beta] \cos(k_r M \bar{R}_h/\beta)}{R_h} d\xi\, d\eta \right\}}_{C_{\bar{\nu}\bar{\mu}}} \quad (8)$$

where

$$C_{\bar{\nu}\bar{\mu}} = R_{\bar{\nu}\bar{\mu}} + iI_{\bar{\nu}\bar{\mu}}$$

$$\bar{\nu}, \bar{\mu} = n - \nu, m - \mu; \text{ respectively}$$

and $\bar{x}, \bar{\xi} = x/b_r, \xi/b_r$; respectively, etc.

In Eq. (8), $C_{\bar{\nu}\bar{\mu}}$ is designated as the complex velocity potential influence coefficient (abbreviated VIC). The integrand of the VIC is of the form $1/R_h$ which has a square root singularity along the forward Mach lines emanating from the receiving point $(x_m, y_n, 0)$. One example of the VIC is shown in Fig. 2 where the freestream Mach number is 1.414 and $k_1 = 0$. The

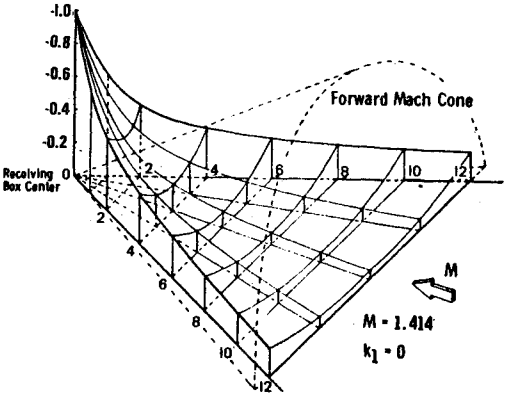


**Fig. 2 Normalized velocity potential influence coefficients.**

value of $C_{\nu\mu}$ is normalized by $C_{oo}$ which is given by a quantity of $(-1)$.

If the planform has a subsonic leading or trailing edge, diaphragms are introduced using Evvard's concept.[3] The diaphragms are artificial surfaces which present no barrier to the flow, across which there can be no pressure discontinuity, and through which continuity of mass is maintained. The upper and lower surfaces of the planform plus diaphragms can now be considered noncommunicative. Thus, $A$ in Eq. (8) is presumed to include any diaphragm regions needed to isolate the upper and lower surfaces. The source distribution placed on the diaphragm is initially unknown, and is evaluated using the boundary condition $\Delta p = 0$ at all points not on the wing surface. Thus, $\Delta\phi = 0$ for an off-wing diaphragm and

$$\Delta\phi(x, y, 0, t) = \Delta\phi(x_{t.e}, y, 0) = \Delta\phi(x_{t,e}, y, 0)\exp[-ik_r(x - x_{t,e})/b_r]e^{iwt} \quad (9)$$

for a diaphragm that lies in the wake of the wing.

According to linear theory, the velocity in the direction normal to the wing (due to the motion of the mean line) is,

$$w(x, y, t) = \frac{\partial z}{\partial t} + U\frac{\partial z}{\partial x} = \sum_{j=1}^{N}\underbrace{\left\{ik_1 z_j(x, y) + b_1\frac{\partial z_j(x, y)}{\partial x}\right\}}_{\bar{w}_j(x, y)\,=\,\text{Dimensionless Upwash}} U\frac{a_j}{b_1}e^{i\omega t} \quad (10)$$

The velocity potential due to the $j$th mode of oscillation will be

$$\Delta\phi_j(x_m, y_n, t) = Ub_1/\beta \times \underbrace{\sum_{\nu}\sum_{\mu}\left\{ik_1 z_j(x, y) + b_1\frac{\partial z_j(x, y)}{\partial x}\right\}C_{\nu\mu}}_{\Delta\bar{\phi}_{j,\,o}}\frac{a_j}{b_1}e^{i\omega t} \quad (11)$$

where $\Delta\bar{\phi}_{j,o}$ = dimensionless potential due to unit amplitude, $a_j/b_1 = 1$.

Once the velocity potential $\Delta\phi_{j,o}$ is evaluated over the surface, the pressure due to the $j$th mode of oscillation is found from the usual linearized expression in the $x, y$ coordinate system

$$P_j(x, y, 0, t) = \rho\frac{D\Delta\phi_j}{Dt} = \rho\frac{U^2}{\beta}\left\{ik_1\Delta\phi_{j,o} + b_1\frac{\partial\Delta\bar{\phi}_{j,o}}{\partial x}\right\}\frac{a_j}{b_1}e^{ik_1\tau} \quad (12)$$

Thus, in the $x, y$ coordinate system (infinitesimal element system) the airloads are evaluated by an integration of the pressure (12) over an area $A(m, n)$

$$L_{j,o}^{m,n} = \rho\frac{U^2}{\beta}\left[ik_1\iint_A\Delta\bar{\phi}_{j,o}(x, y)dxdy + b_1\int\{\Delta\bar{\phi}_{j,o}(x, y)\}\Big|_{x_{l.e}}^{x_{t.e}}dy\right]\frac{a_j}{b_1} \quad (13)‡$$

However, in the box grid system (finite element system) Eq. (13) is numerically integrated over each box assuming at most a linear variation of the velocity potential resulting from the constant pressure over the box area. For example, in the Mach box system,

$$L_{j,o}^{m,n} = \frac{\rho U^2}{2}\frac{b_1^2}{\beta}\frac{2}{\beta}\left[ik_1\Delta\bar{\phi}_{j,o}(x_m, y_n) + \{\Delta\bar{\phi}(x, y_n)\}\Big|_{x_{l.e}^m}^{x_{t.e}^m}\right]\frac{a_j}{b_1} \quad (14)$$

‡ Strictly speaking, $\Delta\phi_{j,o}$ in Eqs. (12) and (13) is evaluated exactly.

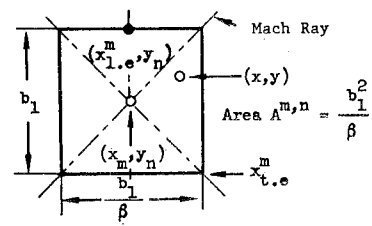


**Fig. 3 Dimensions of Mach box.**

The airload evaluated by Eq. (14) in the transformed Mach box grid system corresponds to the point pressure (12) in the infinitesimal element system. Usually the value obtained from Eq. (14) is represented at the Mach box center as shown in Fig. 3.

The generalized force over the Mach box $(m, n)$ due to deformation in the $i$th elastic or rigid body mode and box loading of the $j$th mode is:

$$Q_{i,j,o}^{m,n}(\omega) = \tfrac{1}{2}\rho U^2\frac{b_1^2}{\beta}\alpha^{m,n}\frac{2}{\beta}\left[ik_1 z_i^{m,n}(x, y)\Delta\bar{\phi}_{j,o}^{m,n} + \frac{1}{\alpha^{m,n}}z_i^{m,n}(x, y)\{\Delta\bar{\phi}^{m,n}(x, y_n)\}\Big|_{x_{l.e}}^{x_{t.e}} - b_1\Delta\bar{\phi}_{j,o}^{m,n}\frac{\partial z_i(x, y)^{m,n}}{\partial x}\right]\frac{a_{j,o}}{b_1} \quad (15)$$

The total generalized force due to all boxes over the wing is

$$Q_{i,j,o}(\omega) = \sum_m\sum_n Q_{i,j,o}^{m,n}(\omega) \quad (16)$$

## Irregular Fluctuation of Airloads and Inflection Points of Velocity Potential Function

In the Mach box grid system, the true leading edge of the planform is replaced by an artificial leading edge. Unless the true leading edge is parallel or perpendicular to the stream flow the artificial leading edge will be jagged as shown in Fig. 4. As may be seen from Fig. 4, leading edges which are not parallel to the Mach rays are represented by an irregular pattern of Mach boxes. It is this irregularity which is the primary cause of the calculated pressure fluctuation. The concept of distortion may be introduced to quantify the irregularity in the relationship between the true and artificial leading edges. This

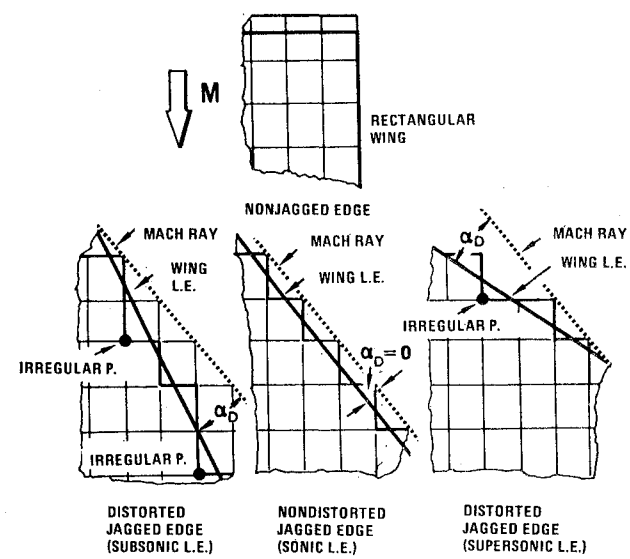


**Fig. 4 Irregularities in distorted jagged leading edges.**

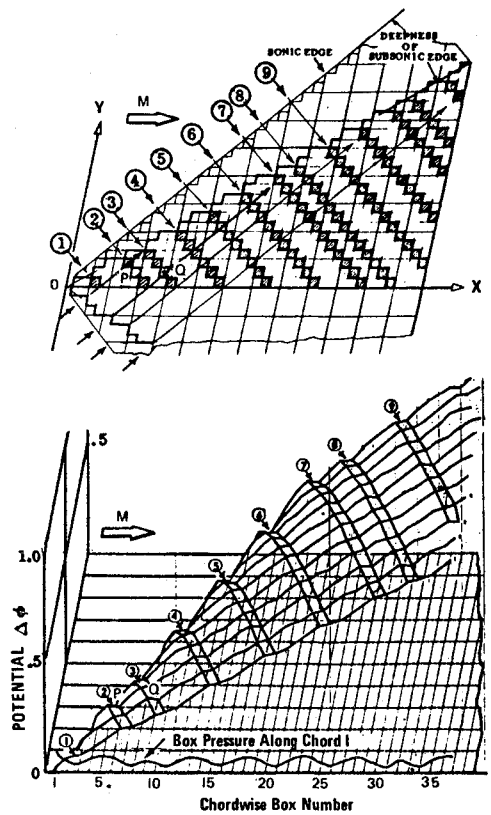


Fig. 5 Inflection points of $\Delta\phi$ and irregular points of wing l.e.

distortion is defined as the maximum distance between the true and artificial leading edges, measured either spanwise or chordwise (whichever is the larger), divided by the box dimension, $b_1$ or $b_1/\beta$, respectively. If the distortion does not exceed one, the planform is nondistorted.

An alternate measure of the distortion is "deepness of subsonic (or supersonic) leading edge," $\alpha_D$, which is defined by the angle between the wing leading edge and the sonic leading edge (which is represented by the off wing diaphragm edge). The $\alpha_D$ for the nondistorted wing leading edge is always zero as shown in Fig. 4.

Another cause is the strong reverse flow on the off wing diaphragm which has a singular behavior along the subsonic leading edge.§ In combination with the previously discussed VIC's, $C_{\overline{\mu\nu}}$, which exhibit square root singularity behavior along the forward Mach lines emanating from the receiving point, a large negative contribution to the velocity potential and box pressure is transmitted along the downstream Mach lines emanating from the irregular points. This is demonstrated by Fig. 5 for the delta wing. The wing is flying at $M = 1.414$ so that the wing leading edge, whose sweepback angle is 57.22°, is completely subsonic. The abscissa represents chordwise Mach box centers and the ordinate indicates $\Delta\phi$. The normal to these axes signifies the chord number counting from the wing center line to the tip. It may be seen that traces of inflection points in the potential, indicated by the circled numbers ①, ②, ... etc., originate from the corresponding irregular points and extend along downstream running Mach rays. The pressure distribution corresponding to the potential distribution along chord 1 is also shown. It can be easily observed that the pressure fluctuation exactly corresponds to the potential inflection tendency. In the case of a mode which is symmetric about the $x$-$z$ plane, an intensified

§ For the supersonic leading edge no diaphragm region exists and the upwash is stepwise discontinuous at the wing leading edge. Therefore, inaccuracies are still caused by the irregular points.

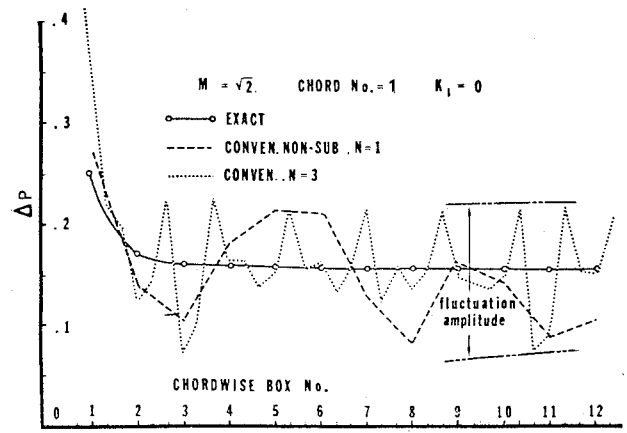


Fig. 6 Chordwise pressure distributions vs increasing in number of Mach boxes.

inflection of $\Delta\phi$ is observed at a point of intersection of both the right and left running Mach rays emanating from irregular points along the right- and left-hand leading edges ($P$ and $Q$ in Fig. 5). Clearly if a finer box grid is chosen, the distortion is unchanged. The geometrical similarity of Mach box patterns at leading edge irregular points is still maintained. Figure 6 shows the pressure distributions along chord number 1 for the original Mach box grid system and for a finer Mach box grid system composed of $N^2(=9)$ times as many boxes. This merely results in increasing the spatial frequency of the pressure fluctuation proportional to the subdivision factor $N$ but does not reduce their amplitudes.

From this discussion, in the case of a sonic leading edge in which the $\alpha_D$ is zero, the pressure irregularity completely vanishes. This is confirmed by Fig. 7. The box pressure computed by Eq. (14) is carried out for a similar delta wing whose leading edge is sonic. The comparison demonstrates that the pressure fluctuation is caused by the irregular points of the wing leading edge which are represented by the deepness of subsonic leading edge, $\alpha_D$.

## Subdivision with Fixed Control Points

In the box grid system, the minimum unit scale is represented by a dimension such as one of the sides or a diagonal of the box. Thus, refinement of the jagged edge is achieved by decreasing

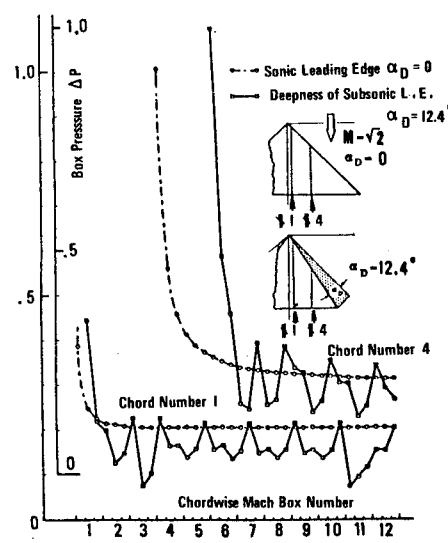


Fig. 7 Chordwise $\Delta P$ for discrete $\alpha_D$ value wings.

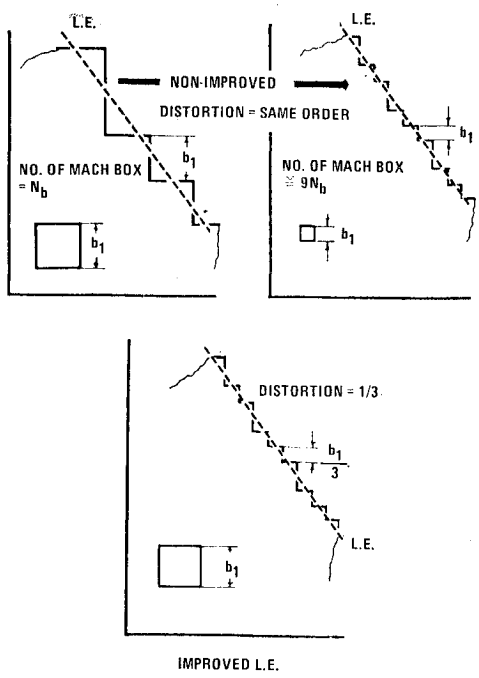


**Fig. 8 Refinement of jagged leading edge in the box grid system.**

the distortion of jagged edge in comparison with the unit standard scale of the box grid system considered. This is illustrated in Fig. 8.

If all the boxes lying on the wing planform and disturbed region are each subdivided into $N^2 = 3^2$ (or $5^2$, etc.) boxes, the center of the large box is coincident with the center of the central sub-box. Since all control points are fixed even after the box grid is subdivided into a finer grid system in odd number increments, the representation of the jagged leading edge is remarkably improved by most effectively avoiding the irregular point effects on the control points (see Fig. 9).

The contribution of each smaller sub-box to each control point is evaluated in the following manner:

1) The upwash at each sub-box can be numerically interpolated from the values at the centers of the large boxes or evaluated by polynomial forms of the modal deformation. The upwash over the off-wing diaphragm, however, varies so rapidly that the interpolation technique is no longer valid.

2) Subdivision is not applied to the whole area. A receiving box is influenced primarily by sending boxes which are close to it. Therefore, there is introduced the concept of effective area which slides from row-to-row in a streamwise direction and contains approximately the same number of sub-boxes as the number of original boxes required in the solution. The influence of those planform boxes which lie outside the effective area will be calculated in the usual manner.

3) The upwash over the off-wing diaphragm is computed at

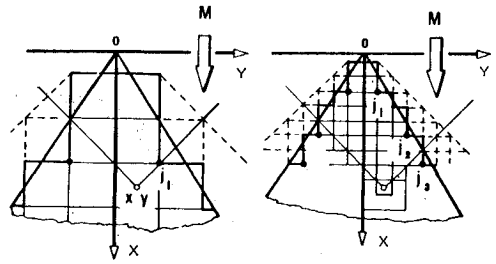


**Fig. 9 Avoidance of irregular points effects by subdivision in odd number increments.**

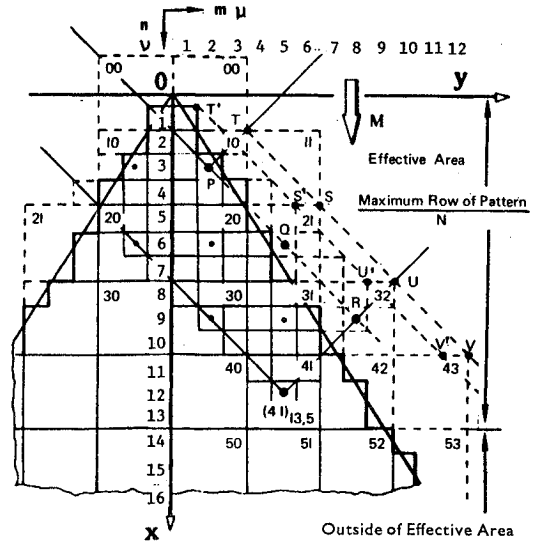


**Fig. 10 Subdivision of box grid system by an odd number 3.**

the center of each sub-box. However, outside the effective area zone, a weighted mean value of the sub-box upwashes over each large box is used to compute the $\Delta\phi$ at the receiving control point. The weighted mean denotes an average, over the large box, of upwashes from both the wing and off-wing diaphragm sub-boxes which are cut by a wing edge.

4) The velocity potential functions evaluated by the above techniques are further smoothed by a least-square error fit method in both spanwise and chordwise directions.

5) Finally, the refined velocity potential functions at each control point on the wing surface are used to compute the aerodynamic loads and generalized forces.

In Fig. 10, for example, the large wing Mach boxes are each subdivided by $3^2$. Before subdivision the dimensionless potential difference at the center of the large box (10), $P$, is evaluated by Eq. (11)

$$\Delta\phi_{(10)} = (b_1/\beta)C_{oo}{}^{(k_1)}w_{10} \qquad (17)\P$$

After subdivision, the potential at the same point will be

$$\Delta\phi_{(10)3,2} = (b_1/3\beta)w_{10}\{C_{oo} + K_{21}C_{11} + K_{11}C_{21} \pm K_{11}C_{22} - (C_{11}/C_{oo})K_{11}\}^{(k_1/3)} \qquad (18)^{**}$$

where $w_{10}$ = upwash over the large box (1, 0) represented at $P$; $K_{ij}$ = interpolation factor at the sub-box $(i, j)$ from the value at the center of the corresponding large box.

A similar calculation may be applied to the upwash over the off-wing diaphragm in the subdivided box grid system. Before the subdivision, the upwash at $Q$ in Fig. 10 is given by

$$w_{21}{}^{(D)} = -(C_{11}/C_{oo})^{(k_1)}w_{10} \qquad (19)$$

After subdivision, the upwash over each diaphragm sub-box is computed in a similar manner by applying the VIC based on $k_1/N$. For example,††

$$w_{(10)22}{}^{(D)} = -K_{11}(C_{11}/C_{oo})^{(k_1/3)}w_{10}$$

For calculation of velocity potential outside the effective area zone, the average upwash is given by a weighted mean value.

¶ Superscript $(k_1)$ denotes the VIC computed at the reduced frequency $k_1$.

** (+) and (−) of the term $K_{11}C_{22}$ correspond to the symmetric and antisymmetric cases of modal input, respectively.

†† Subscript (10) refers to the large box index and sub-subscript 22 refers to the sub-box index in Fig. 10.

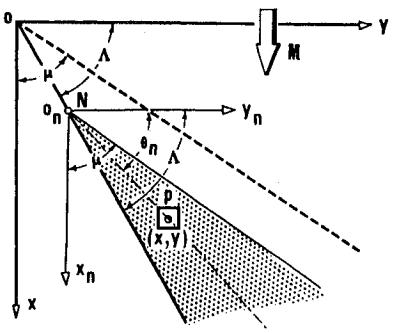


**Fig. 11 L.E. singularity starting at $N$ in the rectangular cartesian coordinate.**

## Singularity Distribution near Subsonic Leading and Side Edges

It is known from the exact solution in steady flow that the upwash over the diaphragm region exhibits a square root singularity, when the subsonic leading and side edges are approached from the outside, which vanishes on the foremost Mach lines. Although it is not clear that the characteristics of the complex upwash in unsteady flow resemble those of the real upwash in steady flow in this flowfield, it is thought to be worth studying the application of a singularity correction to the aerodynamic loadings produced by the subdivision technique described in the previous section. The upwash due to the singularity along the R.H.S. leading edge starting at $(x_N, y_N)$ in Fig. 11 is

$$w(x, y) = (\text{const})W_{SN}\frac{(x - x_N)^{1/2}}{b_r^{1/2}}\frac{1/\beta - \cot\theta_N}{(\cot\theta_N - \cot\Lambda)^{1/2}} \quad (20)‡‡$$

where

$\cot\Lambda$ = wing sweepback angle

$\cot\theta_N = (y - y_N)/(x - x_N)$ = angle of a ray which passes a point $P(x, y)$ with $y_n$ axis

$W_{SN}$ = singularity strength of the L.E. starting at $(x_N, y_N)$.

The leading edge singularity is considered to be linearly superimposed upon each Mach layer (the set of boxes whose diagonals lie on the same Mach ray) and is composed of (Fig. 12), 1) singular distribution of a strength $W_{SO}$ over the region $NOr_o$; 2) singular distribution of a strength $\pm W_{SO}$ over the region $N'Os_o$[(+) and (−) correspond to the symmetric and antisymmetric mode case, respectively]; 3) singular distribution of strength $W_{S1}, \ldots$ over $Nlr_1, \ldots$. The value of $W_{S1}, \ldots$ may be represented as linear combination of incremental addition to $W_{SO}$:

$$W_{S1} = W_{SO} + (\Delta W_{SO})_1 = W_{SO} + \Delta W_{S1}$$
$$W_{S2} = W_{SO} + (\Delta W_{SO})_1 + (\Delta W_{SO})_2 = W_{S1} + \Delta W_{S2} \quad (21)$$

etc.

Each increment of singularity starts at an intersection between the wing leading edge and the sub-box Mach layer as shown 1, ... in Fig. 12.

The total velocity potential difference at $(x_n, y_m)$ is a linear combination of the potential difference due to both the wing surface and leading edge singularities. Therefore,

$$\underbrace{[\Sigma_\nu\Sigma_\mu w(x_\nu, y_\mu)C_\nu}_{(1)} + \underbrace{W_{SO}\Sigma_\nu\Sigma_\mu D_{\nu\mu}{}^{(0)}C_\mu]}_{(2)} = 0 \quad (22)$$

where (1) = induced potential due to upwash on wing; (2) = induced potential due to leading edge singularity; $D_{\nu\mu}{}^{(N)}$ = downwash coefficient in the $N$th Mach layer which is computed by Eq. (20) by applying the numerical values in sub-box system.

In Eq. (22) all values except $W_{SO}$ are known, so the strength of the assumed leading edge singularity starting at 0 is determined at the box center $(x_\nu, y_\mu)$ which is usually chosen at the center of the closest sub-box to the leading edge along the Mach layer. The values on successive sub-boxes along the Mach layer are determined by Eq. (20).

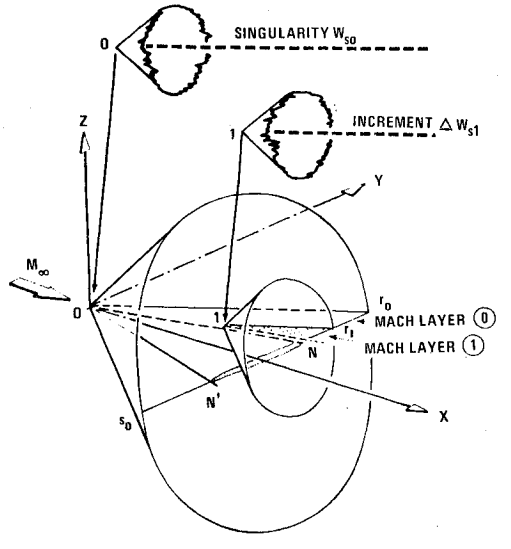


**Fig. 12 Distributed leading edge singularities and sequential Mach layers.**

‡‡ This form of expression is similar to the one applied in Ref. 2.

## Numerical Examples

Numerical examples to demonstrate the effectiveness of the refined method are given. These include steady and unsteady load distributions and aerodynamic coefficients for the delta wing which has been used in the previous sections.

### Steady-State Airloads and Aerodynamic Coefficients

In the steady pitching mode case, the chordwise velocity potential functions for both the conventional and refined Mach box methods are shown in Fig. 13. The refined Mach box

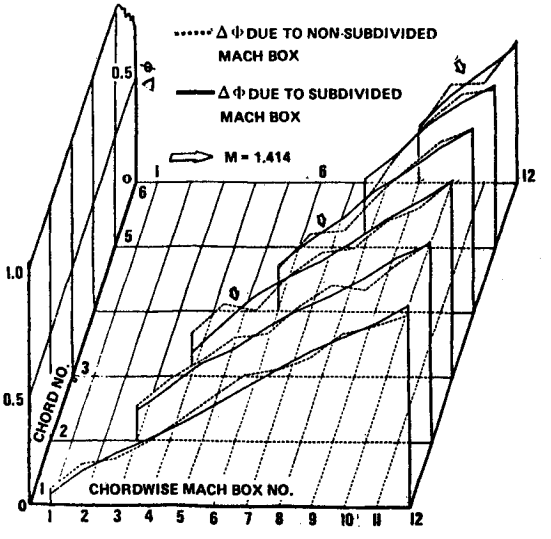


**Fig. 13 Refined and nonrefined chordwise velocity potential functions for case SUB-LED 1-1.**

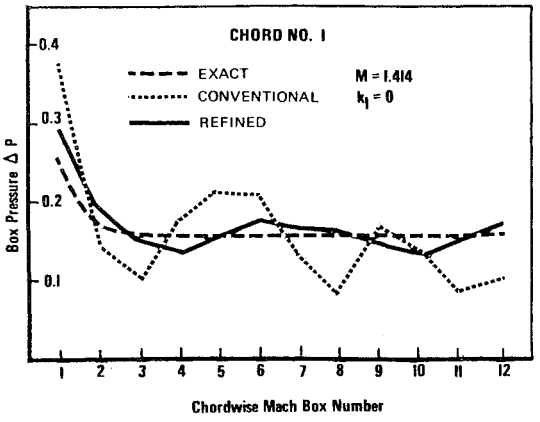


Fig. 14 Box pressure distributions along chord 1 before least squares error fit.

method is performed with a subdivision factor of 3. Even with the least subdivision factor $N = 3$, the velocity potential functions are remarkably improved. An application of the numerical leading edge singularity method is practiced only for this case. Application of this method has indicated only small improvement compared to the method of subdivision with fixed control points. The pressure distributions along chord number 1 which are computed directly from the preceding velocity potential functions with leading edge box area corrections are shown in Fig. 14. It is observed that the refined box pressure distribution is substantially improved relative to the exact pressure distribution. Figure 15 shows the box pressure distributions after applying the Least-Squares-Error Fit (LSEF) technique to the above velocity potential functions. The result shows an excellent agreement between the exact and refined values. On the other hand, the box pressure distribution smoothed from the conventional Mach box method deviates considerably from the exact one. The similar curves which are smoothed by the LSEF method along the chordwise and spanwise directions are plotted in Figs. 16 and 17 for both the refined and conventional Mach box methods. Comparing the results of the refined method to the exact values in these figures, a certain deviation is observed when the chord considered approaches the wing tip. However, these refined values are better than the conventional. This deviation is due to the fact that the delta wing possesses a small number of Mach boxes at the wing tip. The integrated over-all value $C_{L\alpha}$, obtained by the refined method is 2.26 and 1.956 by the conventional method. The exact $C_{L\alpha}$ of the delta wing is 2.42.

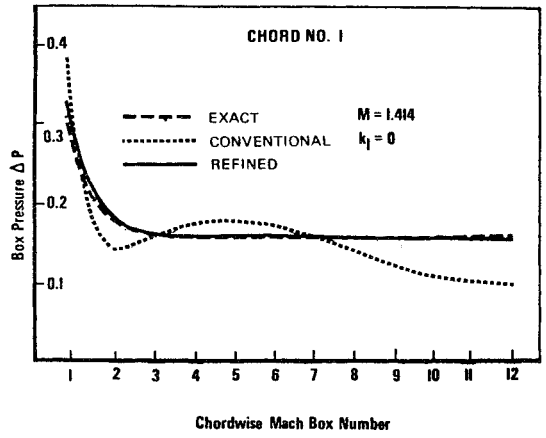


Fig. 15 Box pressure distributions along chord 1 after least squares error fit.

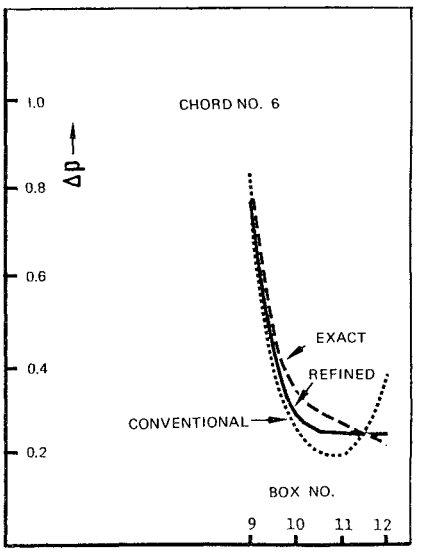


Fig. 16 Box pressure distributions along chord 17 after l. S. E. fit.

### Unsteady Airloads

In contrast to the steady case, there are no analytical methods available for obtaining exact unsteady supersonic airloads on any arbitrary three-dimensional wing with subsonic leading edges, even for cases of upwash involving only rigid body plunging and pitching. An alternate solution for the case of $k_1 \neq 0$, is numerically calculated for the delta wing in which the linearized potential is derived in the form of power series of a frequency parameter, $k_1/M$.[5,6] The unsteady chordwise pressure distributions over the delta wing oscillating in a plunging motion (mode 1) and in a pitching motion (mode

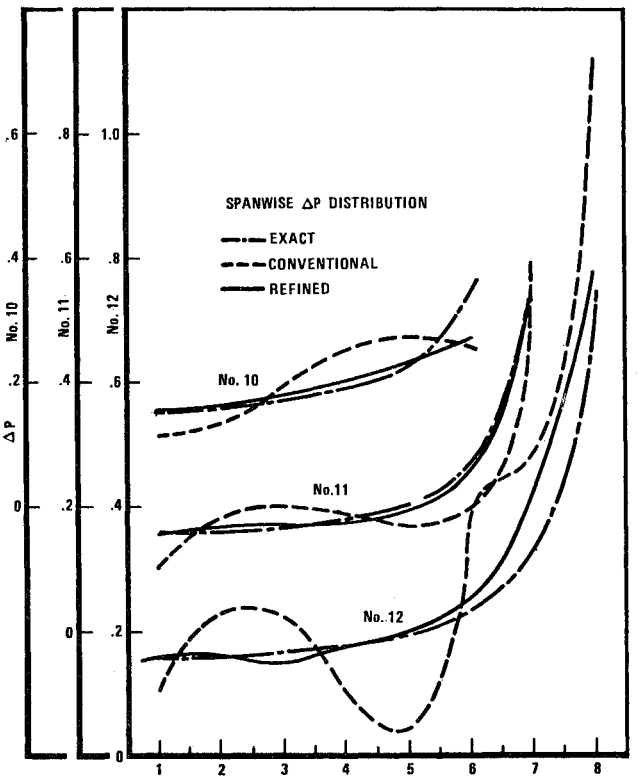


Fig. 17 Spanwise box pressure distributions after least-squares error fit.

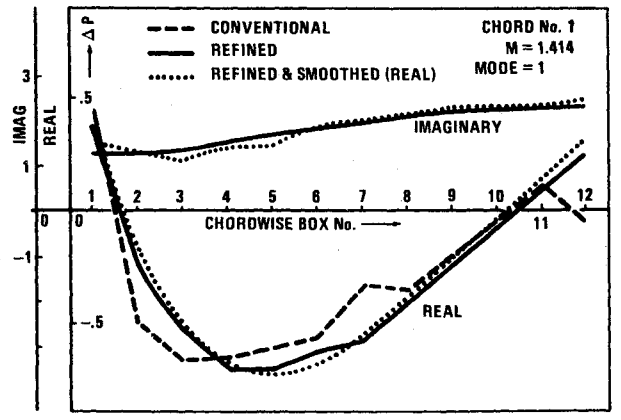


Fig. 18 Box pressure distributions along chord 1 for $k_1 = 0.6$, $M = 1.414$ and mode 1.

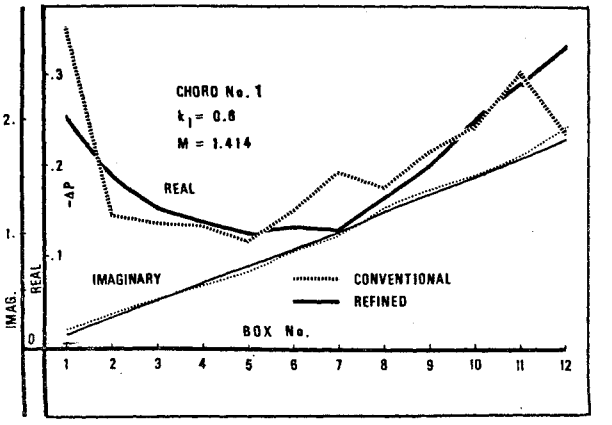


Fig. 19 Box pressure distributions along chord 1 for $k_1 = 0.6$, $M = 1.414$ and mode 1.

2) are shown in Figs. 18 and 19 for both the refined and conventional Mach box methods. Because of the lack of the exact solutions to compare with these results, the index of accuracy is not directly available. A remarkable improvement to the anticipated pressure curves, however, can be detected in these figures from a practical point of view in that a gradual building-up of continuous curves can be expected.

## Concluding Remarks

Theoretical studies to refine the prediction of unsteady aerodynamics of supersonic elastic aircraft have been made. Through these studies, a theoretical interpretation of inaccuracies in the evaluation of airloads by application of the Mach box numerical scheme has been given. These inaccuracies may be significantly reduced by the method of subdivision with fixed control points. An effective-area concept is used to reduce the computing time. The downwash singularity near a subsonic leading edge is also considered. Since it is not clear that the characteristics of the complex upwash for nonzero frequencies resemble those of the real upwash in zero frequency in the wing diaphragm region, this technique is applied only for the steady case. However, results from the numerical singularity method used only in steady case indicate little improvement in accuracy. This is partially due to the fact that even with the present Evvard's method to compute the upwashes over the diaphragm regions, a finely subdivided box grid results in good agreement with the square root singularity velocity profiles. Even with the least subdivision factor $N = 3$, the numerical results of the refined technique show remarkable improvement. In the delta wing tip region where the smallest number of boxes exists, a certain deviation from the exact solution is observed. It is recommended that a higher subdivision factor should be adopted over these critical areas. Also, the subdivision method should be adopted for a wing whose deepness of subsonic (supersonic) leading edge $\alpha_D$ is higher than 5°.

Substantially improved accuracy in the values of load distributions, flutter stability boundaries and dynamic response to continuous turbulence may now be obtained through an application of this method. It is felt that the method can contribute significantly to the prediction of the dynamic behavior of supersonic flight vehicles.

## References

[1] Pines, S., Dugundji, J., and Neuringer, J., "Aerodynamic Flutter Derivatives for a Flexible Wing with Supersonic and Subsonic Edges," *Journal of the Aeronautical Sciences*, Vol. 22, No. 10, Oct. 1955, pp. 693–700.

[2] Zartarian, G. and Hsu, P. T., "Theoretical Studies on the Prediction of Unsteady Supersonic Airloads on Elastic Wings, Pt. I Investigations on the Use of Oscillatory Supersonic Aerodynamic Influence Coefficients," WADC TR 56–97, Dec. 1955, Wright Air Development Center, Ohio; also Zartarian, G., "Pt. II Rules for Application of Oscillatory Supersonic Aerodynamic Influence Coefficients," WADC TR 56–97, Feb. 1956, Wright Air Development Center, Ohio.

[3] Evvard, J. C., "Distribution of Wave Drag and Lift in the Vicinity of Wing Tips at Supersonic Speeds," TN1382, July 1947, NACA.

[4] Andrew, L. V. and Moore, M. T., "Further Developments on Supersonic Aerodynamic Influence Coefficient Methods," *AIAA 6th Structures and Materials Conference*, AIAA, New York, 1965, pp. 203-213.

[5] Watkins, C. E. and Berman, J. H., "Air Forces and Moments on Triangular and Related Wings with Subsonic Leading Edges Oscillating in Supersonic Potential Flow," TR1099, 1952, NACA.

[6] Watkins, C. E. and Berman, J. H., "Velocity Potential and Air Forces Associated with a Triangular Wing in Supersonic Flow, with Subsonic Leading Edges, and Deforming Harmonically According to a General Quadratic Equation," TN 3009, Sept. 1953, NACA.

[7] Donato, V. W. and Huhn, C. R., Jr., "Supersonic Unsteady Aerodynamics for Wings with Trailing Edge Control Surfaces and Folded Tips," AFFDL-TR-68-30, Aug. 1968, Air Force Flight Dynamics Lab., Wright–Patterson Air Force Base, Ohio.